ACS Infectious Diseases

Article

pubs.acs.org/journal/aidcbc

Synergistic Photothermal and Antibiotic Killing of Biofilm-Associated *Staphylococcus aureus* Using Targeted Antibiotic-Loaded Gold Nanoconstructs

Daniel G. Meeker,[‡,∥] Samir V. Jenkins,[†,∥] Emily K. Miller,[†] Karen E. Beenken,[‡] Allister J. Loughran,[‡] Amy Powless,[#] Timothy J. Muldoon,[#] Ekaterina I. Galanzha,[⊥] Vladimir P. Zharov,[⊥] Mark S. Smeltzer,*[,‡] and Jingyi Chen*[,†]

[†]Department of Chemistry and Biochemistry, University of Arkansas, Fayetteville, Arkansas 72701, United States

[‡]Department of Microbiology & Immunology, University of Arkansas for Medical Sciences, Little Rock, Arkansas 72205, United States

[#]Department of Biomedical Engineering, University of Arkansas, Fayetteville, Arkansas 72701, United States

[⊥]Phillips Classic Laser and Nanomedicine Laboratories, University of Arkansas for Medical Sciences, Little Rock, Arkansas 72205, United States

Supporting Information

ABSTRACT: Resistance to conventional antibiotics is a growing public health concern that is quickly outpacing the development of new antibiotics. This has led the Infectious Diseases Society of America (IDSA) to designate *Enterococcus faecium*, *Staphylococcus aureus*, *Klebsiella pneumoniae*, *Acinetobacter baumannii*, *Pseudomonas aeruginosa*, and *Enterobacter* species as "ESKAPE pathogens" on the basis of the rapidly decreasing availability of useful antibiotics. This emphasizes the urgent need for alternative therapeutic strategies to combat infections caused by these and other bacterial pathogens. In this study, we used *Staphylococcus aureus* (*S. aureus*) as a proof-of-principle ESKAPE pathogen to demonstrate that an appropriate antibiotic (daptomycin) can be incorporated into polydopamine-coated gold nanocages (AuNC@PDA) and that daptomycin-loaded AuNC@PDA can be conjugated to antibodies targeting a species-specific surface protein (staphylococcal protein A; Spa) as a means of achieving selective delivery of the nanoconstructs directly to the bacterial cell surface. Targeting specificity was confirmed by demonstrating a lack of binding to mammalian cells, reduced photothermal and antibiotic killing of the Spa-negative species *Staphylococcus epidermidis*, and reduced killing of *S. aureus* in the presence of unconjugated anti-Spa antibodies. We demonstrate that laser irradiation at levels within the current safety standard for use in humans can be used to achieve both a lethal photothermal effect and controlled release of the antibiotic, thus resulting in a degree of therapeutic synergy capable of eradicating viable *S. aureus* cells. The system was validated using planktonic bacterial cultures of both methicillin-sensitive and methicillin-resistant *S. aureus* strains and subsequently shown to be effective in the context of an established biofilm, thus indicating that this approach could be used to facilitate the effective treatment of intrinsically resistant biofilm infections.

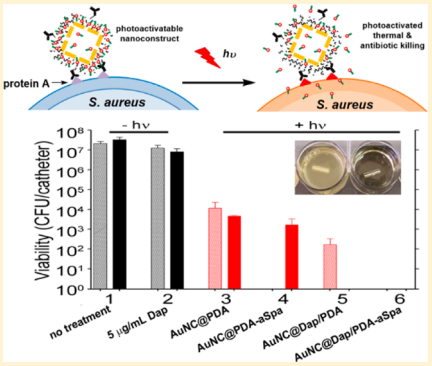

KEYWORDS: *antimicrobial, daptomycin, polydopamine, gold nanocages, methicillin-resistant Staphylococcus aureus, biofilm*

The treatment of bacterial infections has been dramatically compromised by the persistent emergence of antibiotic-resistant strains.[1−3] This growing concern has led the Infectious Diseases Society of America (IDSA) to designate *Enterococcus faecium*, *Staphylococcus aureus*, *Klebsiella pneumoniae*, *Acinetobacter baumannii*, *Pseudomonas aeruginosa*, and *Enterobacter* species as "ESKAPE pathogens" on the basis of the rapidly decreasing availability of antibiotics useful against these pathogens.[4] Although new antibiotics have been developed, the pace of development is slow compared to the emergence of resistant strains. Past experience has also proven that the use of any conventional antibiotic will ultimately lead to the emergence of such resistance.[1] In addition, many forms of bacterial infection, specifically those associated with biofilm formation, are intrinsically resistant to antimicrobial therapy regardless of the acquired resistance status of the offending bacteria.[5] These factors have created an urgent need for the development of alternative antibacterial strategies that would be less subject to the selective forces that drive the emergence of acquired antibiotic resistance.

Two light-activated alternative therapies are photodynamic therapy (PDT) and photothermal (PT) therapy, which employ radically different bactericidal mechanisms from conventional

Received: October 5, 2015
Published: February 10, 2016

DOI: 10.1021/acsinfecdis.5b00117
ACS Infect. Dis. 2016, 2, 241−250

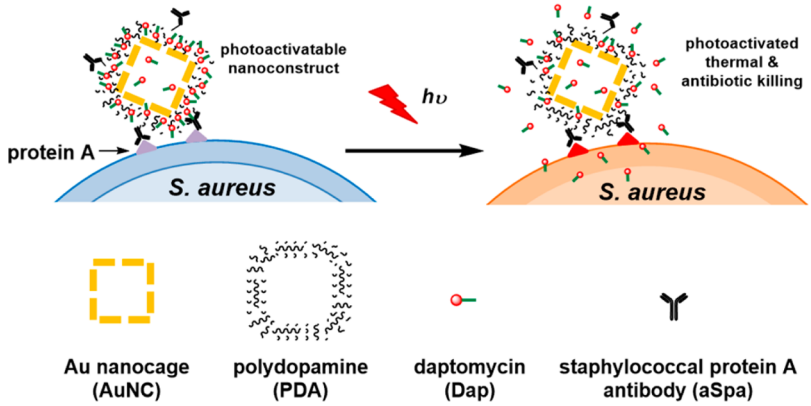

Figure 1. Schematic illustration of the working mechanism of the targeted photoactivatable nanoconstruct for synergistic photothermal and antibiotic treatment of *S. aureus*.

antibiotic therapy.[6] PDT utilizes a photosensitizer and visible light to produce reactive oxygen species (ROS) capable of killing pathogenic microorganisms.[7−9] However, the short lifetimes of ROS present the challenge of adequately damaging enough bacteria to eliminate an infection while not significantly damaging host tissue.[10] We and others have instead explored the use of PT therapy using strong light absorbers such as gold (Au) nanoparticles or carbon nanotubes to generate laser-induced PT effects capable of the targeted physical destruction of bacterial cells.[11−13] Using a murine model, we confirmed that this approach can be combined with photoacoustic flow cytometry to detect and eradicate bacterial cells in the blood.[14,15] Although PT killing alone has great potential to treat bacteremia and has shown some potential in the context of a biofilm,[13] the combined use of PT killing with controlled antibiotic release has the potential to dramatically improve treatment efficacy compared to either therapeutic approach alone. We previously demonstrated that the combined approach of Au nanoparticle-mediated hyperthermia and delivery of tumor necrosis factor cytokines in the context of cancer shows greater therapeutic effects with reduced side effects.[16] Several metal nanoparticle-based medicines are in clinical trials for cancer treatment,[17−19] but to date this combination has not been explored in the context of infectious diseases.

This synergistic approach has tremendous therapeutic promise in that the combination of PT-mediated killing and controlled antibiotic release has the potential to reduce both the laser and antibiotic doses required to achieve the desired clinical effect. To this end, we examined the killing efficacy of a novel pathogen-targeted nanotherapeutic that allowed for both the physical, PT-mediated destruction of bacterial cells and the concomitant release of relatively high concentrations of an antibiotic in the immediate environment of the offending bacterial cells. We chose to focus on *S. aureus* as a proof-of-principle pathogen because of its clinical relevance, antibiotic-resistance status,[3] and prominence as a cause of biofilm-associated infections.[20] The nanoconstructs were made of Au nanocages (AuNCs) coated with polydopamine (PDA) for loading of the antibiotic daptomycin (Dap), which was selected because it is active against methicillin-resistant *S. aureus*[21] and has relatively high efficacy in the context of a biofilm.[22] Dap-loaded nanoconstructs were targeted to *S. aureus* by conjugating antibodies against staphylococcal protein A (aSpa), thereby creating a photoactivatable, highly selective nanodrug. As illustrated in Figure 1, this targeted nanodrug can be activated by near-infrared (NIR) light to convert the photon energy to thermal energy.[23,24] The resulting temperature change is of sufficient magnitude for the simultaneous generation of localized PT effects and expansion of the PDA coating leading to controlled antibiotic release.[25,26] The use of this nanoconstruct to synergize these therapeutic modalities was successfully demonstrated for the methicillin-sensitive *S. aureus* (MSSA) strain UAMS-1 in planktonic culture and, more importantly, for the methicillin-resistant *S. aureus* (MRSA) strain LAC in both planktonic culture and a clinically relevant biofilm model.

METHODS

Synthesis of PDA-Coated AuNCs (AuNC@PDA). The AuNCs were synthesized by galvanic replacement reaction between Ag nanocubes and $HAuCl_4$ as previously described[26,27] and fully detailed in the Supporting Information. AuNC@PDA was prepared by self-polymerization of dopamine on the surface of AuNCs under basic conditions in the presence of O_2. Briefly, 3 mL of 5 nM AuNC aqueous suspension was diluted to 200 mL using Tris-buffered saline (20 mM Tris and 100 mM NaCl, pH 9) in a 250 mL, three-neck, round-bottomed flask. The reaction flask was briefly flushed with O_2 and placed in a bath sonicator held at 4 °C with ice. Dopamine hydrochloride (0.2 mmol, 36.0 mg) was added to the flask, the vessel was sealed under 1 atm of O_2, and the mixture was sonicated throughout the reaction until the extinction peak of AuNC had red-shifted ∼50 nm (∼75 min). After this reaction, the product was collected by centrifugation at 6000 rcf for 10 min, washed with H_2O twice, and recovered by centrifugation at 19,000 rcf for 10 min at 4 °C. The AuNC@PDA was resuspended in H_2O at a concentration of 6 nM for characterization and future use.

Loading of Dap to AuNC@PDA (AuNC@Dap/PDA). Dap was loaded to the AuNC@PDA under different conditions to prepare AuNC@Dap/PDA. Briefly, 1 nM AuNC@PDA was incubated with 1 mg/mL of Dap (0.6 mM) in 1 mL of 10 mM citrate buffer (pH 2.2, 0 mM NaCl; or pH 7.8, 150 mM NaCl). The reaction was allowed to stir overnight at 4 °C in the dark. The product was collected, purified with phosphate-buffered saline (PBS) once and with H_2O three times, and collected by centrifugation at 19,000 rcf for 10 min to remove free Dap. AuNC@Dap/PDA was resuspended in H_2O at a concentration of 4 nM AuNCs for characterization and future use.

DOI: 10.1021/acsinfecdis.5b00117
ACS Infect. Dis. 2016, 2, 241−250

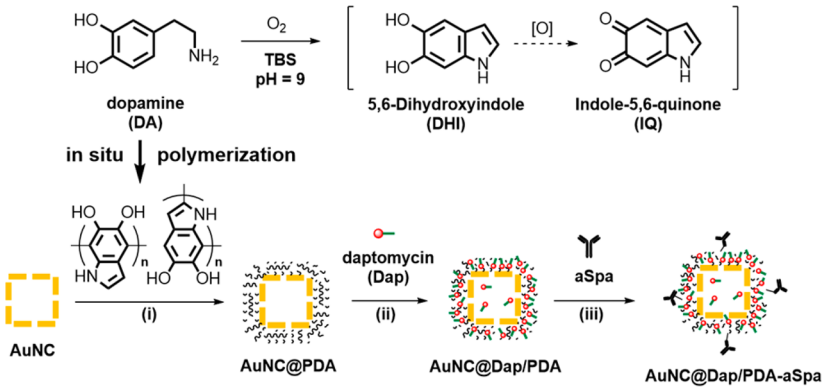

Figure 2. Three-step scheme for synthesis of the nanoconstruct: (i) in situ polymerization of dopamine to form AuNC@PDA; (ii) loading of Dap to obtain AuNC@Dap/PDA; (iii) conjugation of aSpa to yield AuNC@Dap/PDA−aSpa.

Conjugation of aSpa to AuNC@Dap/PDA (AuNC@Dap/PDA−aSpa). aSpa was conjugated to the surface of AuNC@Dap/PDA through the primary amine groups of either the N-terminus or the lysine of the aSpa by Michael addition to form AuNC@Dap/PDA−aSpa. Briefly, 1 nM AuNC@Dap/PDA was dispersed in 1 mL of 10 mM bicene buffer (pH 8.5), and 0.1 nmol of aSpa was added to the solution. The reaction was allowed to proceed at 4 °C for 1 h. The conjugates were collected and washed three times with PBS by centrifugation at 19,000 rcf for 5 min at 4 °C. The conjugates were dispersed in PBS for future use and stored at 4 °C.

Two-Photon Imaging. Cultures of the *S. aureus* strains UAMS-1, LAC, and their isogenic *spa* mutants were grown to an optical density (OD_{560}) of 1.0 in tryptic soy broth (TSB), which corresponds to ~2×10^8 colony-forming units (CFU)/mL. This sample (40 μL) was applied to a glass microscope slide demarcated with a hydrophobic pen and allowed to air-dry. Bacteria were heat fixed before the addition of 90 μL of PBS and 10 μL of AuNC@PDA−aSpa or AuNC@PDA suspension. After 30 min at room temperature, unbound reagents were removed by soaking in PBS three times for 10 min each time. The slide was blotted dry before the addition of 100 μL of 40× diluted 4′,6-diamidino-2-phenylindole (DAPI, NucBlue Fixed Cell ReadyProbe Reagent, Molecular Probes) in PBS and incubation for 10 min. This stain was removed, and the slides were washed by soaking in fresh PBS three times for 5 min each time. The slides were blotted dry, 10 μL of PBS was used as a mounting medium, and a no. 2 coverslip was applied and sealed with nail polish (Saved by the Blue, 230C). Two-photon images were acquired using a customized, four-channel, resonant scanning, multiphoton microscopy platform (Thorlabs, USA) and a 40× water immersion 0.8 NA objective (Nikon). Illumination was provided by a Mai Tai HP ultrafast Ti:sapphire laser (Spectra Physics). DAPI fluorescence was visualized using 10 mW excitation (as measured at the sample) at 700 nm and collecting from blue channel, which utilized a 466 nm center wavelength bandpass with a full width at half-maximum of 60 nm. AuNC luminescence was visualized using 10 mW excitation (as measured at the sample) at 800 nm and collecting from the red channel, which utilized a 607 nm center wavelength bandpass filter with a full width at half-maximum of 70 nm. Images were the average of 200 frames and processed identically using ImageJ (NIH). Quantitative analysis was performed by comparing the ratio of the pixel intensity from AuNC image (800 nm laser, red channel) to the pixel intensity of the DAPI image (700 nm laser, blue channel) in the region of interest. Cells (n = 50) were analyzed, and the intensity ratios were averaged for each sample.

Antimicrobial Activity Analysis. The *S. aureus* strains UAMS-1 and LAC were grown in TSB and diluted to an optical density (OD_{560}) of 0.05, which corresponds to 1×10^7 CFU/mL. TSB was supplemented with 2.5 mM $CaCl_2$, which is required for the in vitro bactericidal activity of Dap. This suspension (180 μL) was placed in each well of a 96-well microtiter plate (1.8×10^6 cells per well). Prior to irradiation, the nanoconstruct suspension for each experimental group was sonicated (Bransonic 2800; Branson) and vortexed for 5 s to ensure homogeneous dispersion. The appropriate nanoconstruct (20 μL of 4 nM in PBS) was then added to each well, giving a final volume of 200 μL and a final AuNC concentration of 0.4 nM, which corresponds to 2.4×10^{11} AuNCs/mL (~2.7×10^4 AuNCs/bacterium). For irradiated groups, the contents of each well were mixed thoroughly, and a Breathe-Easy gas-permeable sealing membrane (Diversified Biotech) was used to seal the microtiter plate prior to irradiation, thus preventing evaporation. Plates containing irradiated groups were placed on ice to slow bacterial growth during the experiment, and each treatment well was irradiated for 10 min by a diode laser (808 nm, 0.75 W) with a 0.30 cm^2 spot size that covered only the surface area of a well. Immediately following irradiation, the sealing membrane was removed, the contents of each well were mixed thoroughly by pipetting, and a 50 μL aliquot was removed for bacterial quantification. For non-irradiated groups, a 50 μL aliquot was removed immediately after mixing for bacterial quantification. After removal of aliquots from each well, plates were resealed and incubated at 37 °C with constant shaking (115 rpm). After 24 h, sealing membranes were removed, the contents of each well were mixed by pipetting, and a 50 μL aliquot was removed for bacterial quantification, which was performed by serial dilution and plate counts to enumerate CFU per well. The analysis of two time points allowed for the simultaneous assessment of PT-mediated killing (quantification at 0 h) and laser-assisted Dap release (quantification at 24 h).

Antimicrobial analysis was also performed with bacteria grown in a biofilm using our previously published model of catheter-associated biofilm formation with slight modifications.[22] Briefly, 14-gauge fluorinated ethylene propylene catheters (Braun, Melsungen, Germany) were cut into 0.5 cm segments, sterilized, and coated in human plasma as previously described.[28] Catheters were then placed in the wells of a 12-well microtiter plate containing 2 mL of TSB supplemented

DOI: 10.1021/acsinfecdis.5b00117
ACS Infect. Dis. 2016, 2, 241−250

with glucose and sodium chloride (biofilm medium, BFM).[28] Each well was then inoculated with the MRSA strain LAC at an OD_{560} of 0.05, and the plate was incubated at 37 °C for 24 h. To treat catheters with our various nanoconstruct formulations, catheters were rinsed in sterile PBS and transferred to the wells of a 96-well microtiter plate. Each well contained 150 μL of BFM supplemented with $CaCl_2$ and 50 μL of the appropriate nanoconstruct (1.2×10^{11} AuNC/well). Controls included catheters placed in 200 μL of BFM and catheters treated with 5 μg/mL of Dap. Catheters were incubated with their respective treatments for 2 h under constant rotation before each catheter was irradiated as described above. Untreated control catheters and catheters exposed to Dap alone were not irradiated. A subset of catheters for each group was harvested immediately and sonicated to disrupt the biofilm. Viable bacteria were subsequently quantified by serial dilution and plate counts. The remaining catheters were allowed to incubate for an additional 24 h at 37 °C in the wells in which they were irradiated, after which they were sonicated and viable bacteria quantified as described for planktonic cultures.

RESULTS AND DISCUSSION

The AuNCs synthesized using the galvanic replacement had outer and inner edge lengths of 55 ± 5 and 38 ± 5 nm, respectively; the localized surface plasmon resonance (LSPR) exhibited an extinction maximum at 753 nm (Figure S1). The AuNCs contained 74% Au and 26% Ag by mass (61% Au and 39% Ag by mole) determined by flame atomic absorption spectroscopy. The targeted antibiotic-loaded nanoconstruct was prepared in three sequential steps following the reaction scheme in Figure 2. First, in situ polymerization of dopamine was used to deposit a layer of PDA on the AuNCs, forming a core–shell structure (AuNC@PDA).[29−31] Next, Dap was stably loaded to the PDA shell through noncovalent interactions to obtain AuNC@Dap/PDA. Finally, aSpa was covalently conjugated to both loaded and unloaded AuNC@PDA via catechol chemistry[32] to yield the nanoconstructs AuNC@PDA–aSpa and AuNC@Dap/PDA–aSpa. Each nanoconstruct was subsequently isolated, purified, characterized, and used to examine bactericidal activity with *S. aureus*.

After polymerization, a layer of PDA with a thickness of 20–50 nm on the AuNC surface was confirmed by TEM (Figure 3A). The hydrodynamic diameter increased from ∼90 nm for AuNCs to ∼200 nm for AuNC@PDA (Figure S2). The LSPR peak shifted to 824 nm (Figure 3B), which was attributed to the change in the refractive index of the medium from 1.33 for water to 1.55 for PDA as the PDA thickness increases.[33,34] During the deposition of PDA, the LSPR maximum of the AuNCs gradually shifted from 753 to 824 nm (Figure S3). The photothermal temperature profile of the AuNC@PDA suspension was measured under the in vitro conditions used for the planktonic studies to determine the therapeutic doses of nanoconstructs and light for in vitro experiments. AuNC@PDA suspensions (200 μL, 0.04–0.4 nM or 2.4×10^{10}–2.4×10^{11} AuNC@PDA/mL) were added to individual wells of a 96-well microtiter plate and irradiated for 10 min using a diode laser centered at 808 nm with output power of 0.75 or 0.38 W (1.67 or 0.83 W/cm^2, ∼30% power loss through the film cover), which covered the entire surface area of the well (0.3 cm^2). The increase in temperature plateaued after ∼5 min and, as expected, the change in temperature was dependent on both AuNC@PDA concentration and laser fluence (Figure 3C,D).

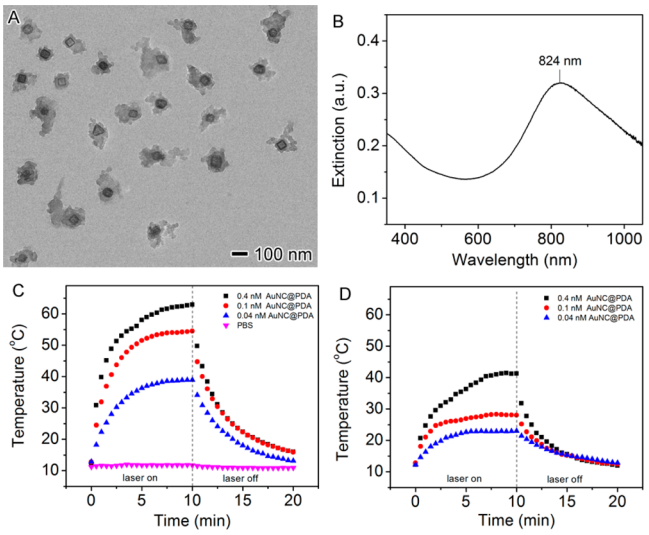

Figure 3. (A) TEM image of AuNC@PDA. (B) UV–vis–NIR spectrum of AuNC@PDA aqueous suspension. (C, D) Temperature profile of 200 μL AuNC@PDA suspensions in PBS at concentrations of 0.04 nM (blue triangles), 0.1 nM (red circles), and 0.4 nM (black cubes) as a function of irradiation time using an 808 nm diode laser at power density of (C) 1.67 W/cm^2 and (D) 0.83 W/cm^2.

Killing efficacy of different AuNC nanoconstructs was assessed using a 96-well microtiter plate format. Unless otherwise noted, 1.8×10^6 *S. aureus* cells and the treatment of interest were combined in a final volume of 200 μL per well. In the control experiments carried out to establish a baseline for these studies, the *S. aureus* strain UAMS-1 was seeded, and aliquots were removed at 0 and 24 h for bacterial cell viability analysis by plating on growth medium tryptic soy agar (TSA) to determine the number of CFU. The immediate (0 h) studies confirmed the initial concentration of bacteria, whereas a sample taken after 24 h of incubation at 37 °C showed a concentration of 10^9 CFU/mL (Figure 4, group 1). Because

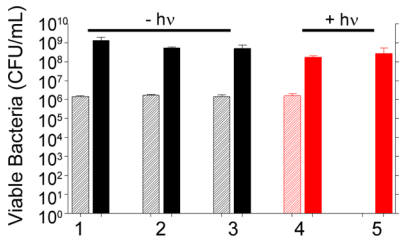

Figure 4. Bacterial cell killing of various formulations against *S. aureus* investigated 0 h (striped bars) and 24 h (solid bars) following treatment: (1) no treatment; (2) 0.4 nM AuNC; (3) 0.4 nM AuNC@PDA; (4) laser irradiation; (5) 0.4 nM AuNC@PDA and laser irradiation. Killing was assessed at 0 h (striped bars) and 24 h (solid bars) post treatment. Black bars indicate non-irradiated groups, and red bars indicate irradiated groups.

AuNCs contain some residual Ag, a known antimicrobial, uncoated AuNCs were incubated at 0.4 nM (4.8×10^{10} AuNC/well, $\sim 2.7 \times 10^4$ AuNC/cell), and no significant bacterial death was observed (Figure 4, group 2). Similarly, exposure to AuNC@PDA showed no decrease in CFU (Figure 4, group 3), and irradiation in the absence of AuNCs had no effect on viability (Figure 4, group 4). When AuNC@PDA was combined with 808 nm diode irradiation, a reduction in

DOI: 10.1021/acsinfecdis.5b00117
ACS Infect. Dis. 2016, 2, 241–250

CFUs below the limit of detection (20 CFU/well) was observed for the 0 h time point, but the number of viable cells rebounded to control levels by the 24 h time point (Figure 4, group 5). These results confirm the ability to photothermally kill bacterial cells under these conditions, but also illustrate that the PT effect alone is not sufficient to completely eradicate viable bacteria under these test conditions.

To assess the synergistic effect of antibiotic release, we next assessed bacterial killing using Dap-loaded AuNC@PDA. Loading of Dap to the PDA coating was achieved through noncovalent interactions. The zeta potential of AuNC@PDA is neutral at a pH ~3.0 and, as expected, changes from negative to positive as pH decreases (Figure 5A). Using a fixed concentration of 0.6 mM, Dap was loaded to AuNC@PDA at pH 7.8 or 2.2. The loading capacities of Dap were found to be 4 μg/mL at pH 7.8 and 16 μg/mL at pH 2.2 in 0.4 nM AuNC@PDA (6.2×10^3 and 2.5×10^4 Dap per AuNC@PDA), referred to as AuNC@Dap_{Lo}/PDA and AuNC@Dap_{Hi}/PDA, using ultraperformance liquid chromatography (UPLC) by integrating the area of daptomycin elution at ~3.5 min (Table S1 and Figure S4A). The light-triggered release of Dap was then examined under the in vitro irradiation conditions described above (Figure 5B).

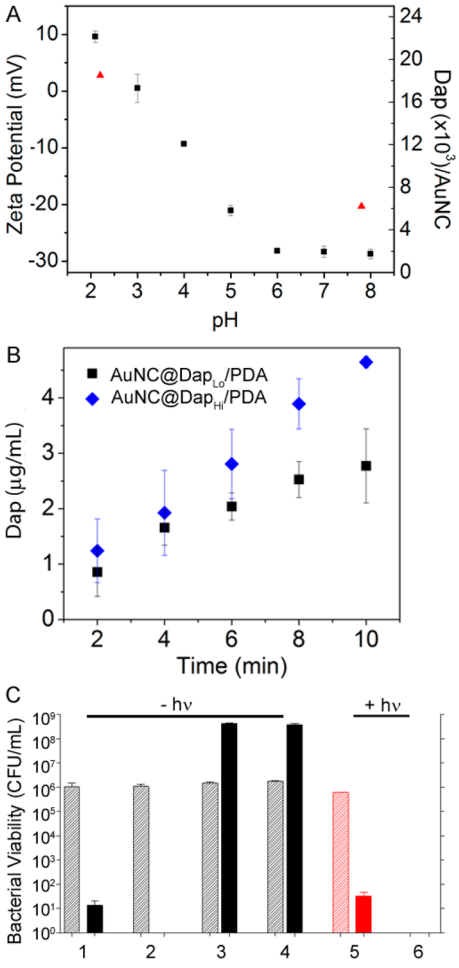

Figure 5. (A) Zeta potential of AuNC@PDA (squares) and loading capacity of Dap (triangles) as a function of pH value. (B) Release profiles of Dap upon irradiation by a diode laser at 808 nm with a power density of 1.67 W/cm^2 at a concentration of 0.4 nM AuNCs with different Dap loadings: 4 μg/mL or 6.2×10^3 Dap molecules per AuNC (AuNC@Dap_{Lo}/PDA, squares) and 16 μg/mL or 2.5×10^4 Dap per AuNC (AuNC@Dap_{Hi}/PDA, diamonds). (C) Bacterial killing without irradiation and treatment of (1) 2 μg/mL Dap, (2) 5 μg/mL Dap, (3) AuNC@Dap_{Lo}/PDA (4 μg/mL), and (4) AuNC@Dap_{Hi}/PDA (16 μg/mL) and with irradiation (5) 2 μg/mL Dap and (6) AuNC@Dap_{Lo}/PDA (4 μg/mL, 2 μg/mL released). Killing was assessed at 0 h (striped bars) and 24 h (solid bars) post treatment. Black bars indicate non-irradiated groups, and red bars indicate irradiated groups.

The nanoconstructs were stable for at least 3 months at 4 °C in PBS, with the amount of Dap released into solution during that time below the quantification limit of UPLC (<1 μg/mL). The corresponding temperature profiles of the samples showed that the suspension temperature rapidly increased above 37 °C within 1−2 min of irradiation and reached a plateau at ~55 °C after 5 min of irradiation (Figure 3). Within the first 2 min, the amount of Dap released was ~1 μg/mL with release continuing through the 10 min irradiation period (Figure 5B). To rule out leakage at physiological temperature, the samples were incubated at 37 °C for 24 h, and the amount of Dap released remained ~1 μg/mL. The binding experiment was performed by varying the Dap concentration at a fixed concentration of AuNC@PDA (1 nM), and the bound Dap per 1 nM AuNC@PDA was plotted as a function of the total concentration of Dap (Figure S6). The interactions of Dap to AuNC@PDA were further analyzed by Scatchard method. The result suggests a biphasic binding involving strong interactions including electrostatic interactions, hydrogen bond, π stacking, and perhaps covalent interactions, as well as weak interactions such as hydrophobic interactions.[35] Additionally, Dap is a cyclic lipopeptide (13-mer)[36] having an isoelectric point (pI) of ~3.8,[37] and has been found to aggregate via a pH-dependent reversible "self-association" mechanism.[38] The increase in loading capacity at low pH is attributable to self-association of Dap. These noncovalent interactions are reversible at elevated temperature, thus facilitating the photothermal release of Dap.[38,39]

As a control for the antibacterial activity of Dap, *S. aureus* cells were incubated with Dap at 2 or 5 μg/mL, which represent 2 and 5 times the Clinical Laboratory Standards Institute (CLSI)-defined breakpoint minimum inhibitory concentration (MIC) used to define a Dap-sensitive strain of *S. aureus*.[22] In the absence of laser irradiation, concentration-dependent killing was observed after 24 h of exposure, with 5 μg/mL being sufficient to eradicate the sample of viable bacteria (Figure 5C, groups 1 and 2). In the absence of irradiation, AuNC@Dap_{Lo}/PDA (4 μg/mL Dap loaded, <1 μg/mL released Dap in the well) and AuNC@Dap_{Hi}/PDA (16 μg/mL Dap loaded, <1 μg/mL released Dap in the well) did not result in any appreciable cell killing irrespective of the amount of Dap loaded (Figure 5C, groups 3 and 4), confirming the lack of Dap release from the polymer. With irradiation, exposure to 2 μg/mL Dap showed no effect at 0 h and a comparable reduction in viable bacteria (Figure 5C, group 5) to that observed with the same concentration of Dap in the absence of laser irradiation (Figure 5C, group 1). This demonstrates that laser irradiation does not reduce the antimicrobial activity of Dap. In contrast, laser irradiation in combination with AuNC@Dap_{Lo}/PDA at the same Dap concentration reduced the number of viable bacterial cells below the limit of detection at both 0 and 24 h post-treatment (Figure 5C, group 6).

Although these results confirm bacterial cell killing with Dap-loaded AuNC@PDA nanoconstructs, they must be interpreted in the context of the confined environment of the wells of a

DOI: 10.1021/acsinfecdis.5b00117
ACS Infect. Dis. 2016, 2, 241−250

microtiter plate. For the transition to in vivo use, some means of localization is likely to be required as a means of targeting the offending bacterial cells within the complex milieu of the host. To address this, we conjugated aSpa to the surface of AuNC@PDA via Michael addition[40] between the primary amines and the aromatic rings (Figure 6A) to yield AuNC@PDA−aSpa. The reaction site of the conjugation is postulated to be either N-terminus or the lysine of the aSpa. The number of aSpa molecules on the nanoconstruct surface was quantified using a Dylight488-labeled secondary IgG antibody (caprine, antilapine) following KCN dissolution of AuNCs. An average of 19 antibodies per AuNC@PDA was determined by fluorescence intensity of the Dylight488-labeled IgG (λ_{ex} = 493; λ_{em} = 518 nm) with calibration curve and results shown in Figure S4C,D. The irradiation profile of AuNC@PDA−aSpa is similar to that of AuNC@PDA (Figure S5). On the basis of CFU counts at the immediate time point, we achieved a 2−3 log reduction in CFU following irradiation of UAMS-1 treated with AuNC@PDA−aSpa, which was attributed to PT effects (Figure 6B, group 2). This effect was apparent only at the immediate time point, with CFU counts rebounding at 24 h to levels like those observed in the untreated control group (Figure 4, group 1) and the non-irradiated group exposed to the same nanoconstruct (Figure 6B, group 1). These same trends were also observed with the MRSA strain LAC. Specifically, a decrease in CFU of 3−4 logs was observed immediately after irradiation followed by a rebound to untreated levels at 24 h (Figure 6B, group 3).

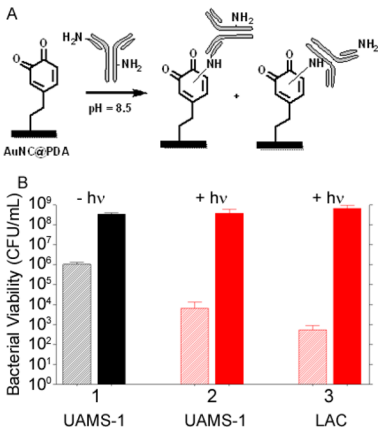

Figure 6. (A) Reaction scheme for conjugation of aSpa to AuNC@PDA. (B) Bacterial cell killing using AuNC@PDA−aSpa against UAMS-1 (1) without irradiation, (2) with irradiation, and (3) against LAC with irradiation. Killing was assessed at 0 h (striped bars) and 24 h (solid bars) post treatment. Black bars indicate non-irradiated groups, and red bars indicate irradiated groups.

Binding of the aSpa functionalized nanoconstructs to *S. aureus* was confirmed by two-photon luminescence imaging of *S. aureus* cells exposed to AuNC@PDA−aSpa by comparison to those exposed to AuNC@PDA and unexposed cells. *S. aureus* cells stained with DAPI appeared only in the blue channel, whereas the spectrally broad AuNC emission was strongest in the red channel.[41] Color was added during postprocessing to yield the composite images, and pixel intensity was quantified for both DAPI and AuNC frames (Figure S7). These studies were done with the MSSA strain UAMS-1 and the MRSA strain LAC, which are genetically and phenotypically distinct. Of particular note, UAMS-1 produces protein A at high levels relative to LAC.[42−44] For both UAMS-1 and LAC, the results showed colocalization of red and blue signals with *S. aureus* cells exposed to AuNC@PDA−aSpa (Figure 7A,D), suggesting that AuNC@PDA−aSpa attached to the cell surface. No colocalization was observed with *S. aureus* cells exposed to AuNC@PDA (Figure 7B,E).

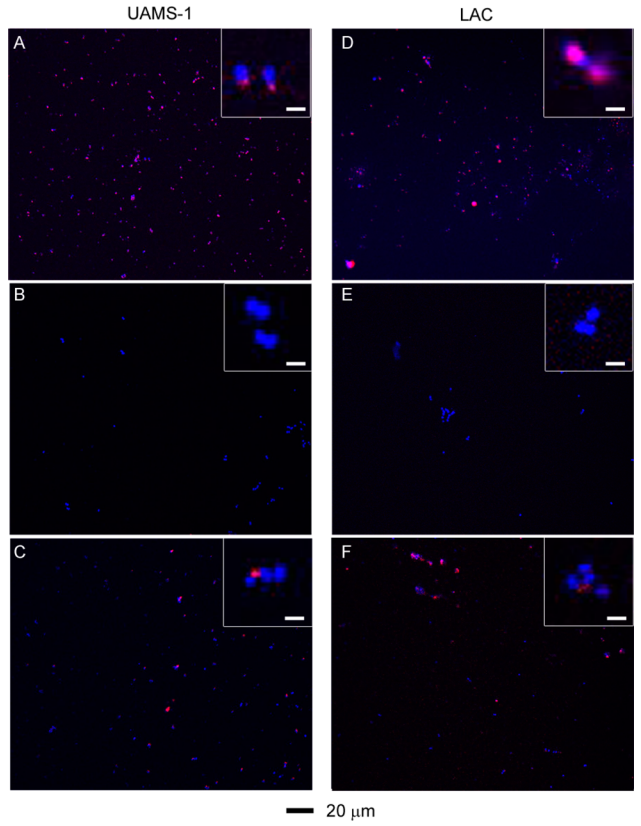

Figure 7. Two-photon fluorescence images of *S. aureus* cells treated at different conditions: (A) UAMS-1 exposed to AuNC@PDA−aSpa; (B) UAMS-1 exposed to AuNC@PDA; (C) UAMS-1 *spa* mutant exposed to AuNC@PDA−aSpa; (D) LAC exposed to AuNC@PDA−aSpa; (E) LAC treated with AuNC@PDA; (F) LAC *spa* mutant exposed to AuNC@PDA−aSpa. Cells were stained with DAPI colored in blue. Luminescence of AuNCs was colored in red.

As an additional control, isogenic *spa* mutants that do not produce protein A were also examined in these experiments (Figure 7C,F). Surprisingly, colocalization was observed, which is likely due to the antibody binding to other proteins on the cell surface. Western blotting of conditioned medium using the same aSpa antibody revealed the presence of additional reactive proteins in both the UAMS-1 and LAC *spa* mutants (Figure S8). In this respect it should be emphasized that Spa is an IgG-binding protein and that *S. aureus* is known to produce other such proteins, one example being Sbi.[45] Although this somewhat complicates interpretation of these results, in the context of the therapeutic approach we propose, binding of aSpa to multiple *S. aureus* biomarkers is advantageous as it would further enhance antibody targeting, particularly in strains that produce relatively low levels of Spa. Additionally, we confirmed the absence of binding to human endothelial cell line EA-hy926, thus suggesting that the use of aSpa as a targeting agent is unlikely to be associated with mammalian cell toxicity (Figure S9).

DOI: 10.1021/acsinfecdis.5b00117
ACS Infect. Dis. 2016, 2, 241−250

Following Dap loading at 4 and 16 μg/mL, aSpa was conjugated to the AuNC@Dap/PDA nanoconstructs. The numbers of aSpa per AuNC@Dap/PDA were determined to be 28 and 13, respectively, which are comparable to those observed with AuNC@PDA without Dap loading (Figure S4). No bacterial cell killing was observed without irradiation (Figure 8, groups 1 and 2), but irradiation of UAMS-1 treated

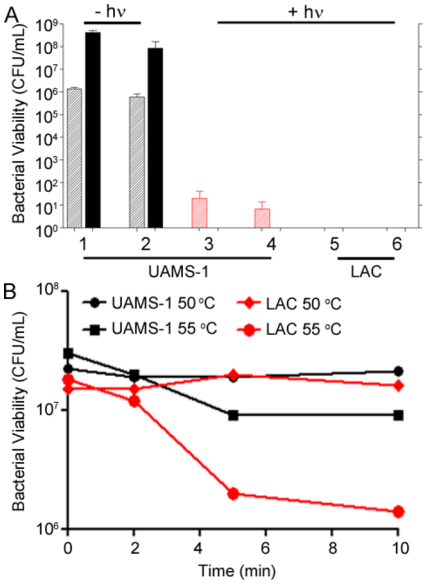

Figure 8. (A) Bacterial cell killing of UAMS-1 (groups 1–4) using AuNC@Dap/PDA–aSpa at low (4 μg/mL, groups 1 and 3) and high (16 μg/mL, groups 2 and 4) daptomycin loading without (groups 1 and 2) and with (groups 3 and 4) irradiation assessed at 0 (striped bars) and 24 h (solid bars) after treatment. Results are also shown for studies done with LAC after laser irradiation using AuNC@Dap/PDA–aSpa with Dap at low (group 5) and high concentrations (group 6). Black bars indicate non-irradiated groups, and red bars indicate irradiated groups. (B) Thermal kill curves of UAMS-1 (black) and LAC (red) at 50 and 55 °C.

with either AuNC@Dap/PDA–aSpa formulation completely eliminated the rebound of bacterial growth observed with AuNC@PDA–aSpa (Figure 8, groups 3 and 4). These results indicate that the combination of Dap release from the nanoconstruct and photothermal treatment has a synergistic effect by comparison to exposure to Dap or PT killing alone. Eradication of viable bacteria at 24 h was apparent at both Dap concentrations, further emphasizing the therapeutic synergy of our approach. The same effect was also observed with the MRSA strain LAC, but LAC appeared to be even more sensitive to PT-mediated killing than UAMS-1. Specifically, with Dap loading the number of viable bacteria was below the level of detection at both the immediate and 24 h time points (Figure 8, groups 5 and 6). These results suggest that LAC is more thermally sensitive than UAMS-1 in the relevant temperature range of 50–55 °C, which was subsequently confirmed in experiments that exposed either strain to 50 or 55 °C with samples removed at 2 min intervals to assess the decrease in CFU (Figure 8B). The mechanism for this, or whether it is a consistent distinction between MSSA and MRSA strains, remains to be determined.

We subsequently confirmed that at a fixed volume (200 μL) decreasing the concentration of AuNC@Dap/PDA–aSpa while holding the number of bacterial cells constant or increasing the number of bacterial cells while holding the concentration of AuNC@Dap/PDA–aSpa constant both resulted in a corresponding decrease in bacterial cell death (Figure S10). This was true at both the immediate and 24 h time points, thus confirming a concentration-dependent effect in the context of both PT-mediated killing and antibiotic release. Importantly, studies done with surviving bacterial cells after exposure to AuNC@Dap/PDA–aSpa and irradiation confirmed no change in MIC (data not shown), thus demonstrating that these relationships are in fact a function of the overall concentration of AuNC@Dap/PDA–aSpa as reflected in our thermal curves as well as the number of AuNC@Dap/PDA–aSpa per bacterial cell.

We also confirmed that both the PT and antibiotic killing effects with our AuNC@Dap/PDA–aSpa nanoconstructs were reduced in a concentration-dependent manner in the presence of unconjugated aSpa (Figure S11). This confirms the targeting specificity of our approach and demonstrates that the synergistic killing effects we observed are greatly enhanced by localization of AuNC@Dap/PDA–aSpa to the bacterial cell surface rather than generalized effects associated with PT effects and antibiotic release within the confined environment of a microtiter plate well. Further support for this hypothesis, as well as for the targeting specificity of our AuNC@Dap/PDA–aSpa formulation, comes from the observation that the killing effects we observed were greatly attenuated when the experiments were repeated with *Staphylococcus epidermidis*, a staphylococcal species that does not produce protein A (Figure S12). Specifically, a concentration of AuNC@Dap/PDA–aSpa of 0.4 nM was not sufficient to achieve 100% killing of *S. epidermidis* (Figure S12), whereas a concentration of only 0.2 nM was sufficient for this purpose with *S. aureus* (Figure S10A). Presumably, given that *S. epidermidis* does not produce Spa or any other recognized IgG-binding protein, what killing was observed with *S. epidermidis* was likely due to generalized effects of the confined microtiter plate environment.

Finally, although a novel means of killing bacterial cells at a single cell level is important in an era of increasing antibiotic resistance, many bacterial infections, including those associated with the formation of a biofilm, are intrinsically resistant to antibiotic therapy irrespective of the acquired resistance status of the offending strain.[46] Because of the clinical importance of infections caused by MRSA strains, we tested the efficacy of our nanotherapeutic approach against LAC in the context of established *S. aureus* biofilms. Biofilms were grown onto 0.5 cm segments of catheters and then exposed to the various formulations described above. As would be expected given the intrinsic resistance of a biofilm, exposure to 5 μg/mL Dap had only a modest impact on the number of viable bacteria per catheter by comparison to the untreated controls (Figure 9, groups 1 and 2). After laser irradiation, exposure to untargeted AuNC@PDA resulted in a several log reduction of CFU at 0 and 24 h (Figure 9, group 3). Targeting with aSpa increased the PT effect as determined immediately after irradiation but, in the absence of Dap loading, did not completely eradicate viable bacteria from the biofilm (Figure 9, group 4). Whereas exposure to 5 μg/mL Dap had only a modest impact on bacterial viability within the biofilm (Figure 9, group 2), a clear PT effect was observed after laser irradiation of bacteria exposed to AuNC@Dap_{Hi}/PDA, and no viable bacteria were detected at the 24 h time point (Figure 9, group 5). These results confirm that the synergistic effects of PT killing and daptomycin release observed in planktonic cultures were also

DOI: 10.1021/acsinfecdis.5b00117
ACS Infect. Dis. 2016, 2, 241–250

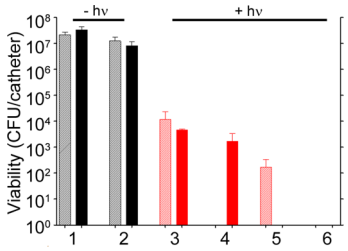

Figure 9. Bacterial cell killing using a biofilm model. Experimental groups are (1) no treatment, (2) 5 μg/mL Dap, and irradiation plus (3) AuNC@PDA, (4) AuNC@PDA−aSpa, (5) AuNC@Dap_{Hi}/PDA, and (6) AuNC@Dap_{Hi}/PDA−aSpa. Killing was assessed at 0 h (striped bars) and 24 h (solid bars) after treatment. Black bars indicate non-irradiated groups, and red bars indicate irradiated groups.

apparent in the context of an established biofilm. Moreover, when biofilms were exposed to AuNC@Dap_{Hi}/PDA−aSpa and irradiated, no viable bacteria were detected at either the immediate or 24 h time points (Figure 9, group 6). These results strongly support the hypothesis that the synergistic effects of PT killing and targeted antibiotic release are more effective than either therapeutic approach alone, even in the context of an established biofilm.

CONCLUSION

We developed a polymer-coated, antibiotic-loaded, antibody-targeted, Au-based nanoconstruct and used *S. aureus* as a proof-of-principle pathogen to demonstrate that photothermal heating can be combined with antibiotic delivery for the synergistic treatment of bacterial infections. Specifically, PDA-coated AuNCs were incubated with *S. aureus* and irradiated to induce PT heating. Immediately after PT treatment, a several log reduction in viable bacteria was observed, but after 24 h, the bacterial population had increased back to control levels. However, this effect was not observed when the experiments were done with laser-irradiated, daptomycin-loaded AuNC@PDA. Thus, by combining these two components we confirm the ability to reduce bacterial viability immediately after irradiation due to PT killing and to completely eradicate viable bacteria at 24 h owing to antibiotic-mediated effects. We also confirm that effective targeting to bacterial cells can be achieved using appropriate antibodies. We chose anti-Spa (aSpa) as our "proof-of-principle" antibody because protein A is a characteristic protein produced by essentially all strains of *S. aureus*, albeit in various levels.[47] We also confirmed the targeting specificity of aSpa using a mammalian cell line, the Spa-negative bacterial species *S. epidermidis*, and the use of blocking aSpa antibodies. This does not preclude the use of alternative *S. aureus* targeting agents either alone or in combination with aSpa, which is an area of active investigation. Additionally, overall targeting specificity remains to be determined in the context of both other bacterial species that produce IgG-binding proteins (e.g., *Streptococcus pyogenes*) and potentially even other human cell types. However, the primary emphasis in these experiments was on evaluating our antibiotic-loaded AuNC nanoconstruct and determining the feasibility of using antibodies as targeting agents to achieve the desired synergistic effects, and the results we report definitively demonstrate the feasibility of this approach. The applicability of our system could be extended to other bacterial species by changing the targeting agent and potentially the antibiotic. Moreover, the results we present confirm that we can achieve these synergistic effects even in the context of an established biofilm and that, by doing so, viable bacteria can be eliminated from the biofilm at least under the in vitro test conditions employed here. Indeed, in the context of an established *S. aureus* biofilm, complete eradication of viable bacteria was achieved only using the targeted, drug-loaded, irradiated nanoconstruct.

The ultimate goal is to develop a broadly applicable nanotherapeutic approach capable of eradicating viable bacteria, including those that exhibit acquired antibiotic resistance or are intrinsically resistant owing to their presence within a biofilm, without causing collateral damage to the human host. Thus, the obvious challenge now is to evaluate and optimize our approach under in vivo conditions and expand our approach to other bacterial pathogens. For instance, one potential application of the approach we describe would be in the context of orthopedic infections following traumatic injury and/or surgical debridement of the infected site. In such cases, the surgeon would have direct access to the site, thus greatly facilitating laser irradiation, and this has the potential to limit both the development of infection and the extent of debridement required to ensure complete eradication of an established infection, particularly when employed in the context of concomitant systemic antibiotic therapy. This is a particularly important consideration in that the surgeon is often presented with a "catch-22" in which the likelihood of eradication is greatly enhanced by an extensive debridement, but at the same time such debridements often create structurally unstable defects that require subsequent reconstructive surgeries that themselves present an additional opportunity for infection.[48] Thus, although much remains to be addressed, our results nevertheless provide the necessary experimental foundation to pursue these studies in the context of diverse bacterial pathogens and diverse forms of bacterial infection, including those associated with biofilm formation.

ASSOCIATED CONTENT

Supporting Information

The Supporting Information is available free of charge on the ACS Publications website at DOI: 10.1021/acsinfecdis.5b00117.

Experimental details, TEM and UV−vis spectra of AuNCs, DLS data, UV−vis spectra of the polymer coating process and the LSPR shift profile, UPLC calibration curve and data analysis, UV−vis spectra of nanoconstructs, fluorescence calibration, and data analysis, temperature profile of PT effects, Scatchard plot, quantitative analysis of two-photon fluorescence images, Western blot analysis of *spa* mutants, images of targeting specificity study on human cells, and dose response curve of the photoactivated nanoconstructs (PDF)

AUTHOR INFORMATION

Corresponding Authors

*(J.C.) E-mail: chenj@uark.edu (nanoconstructs).
*(M.S.S.) E-mail: SmeltzerMarkS@uams.edu (bacteriology).

Author Contributions

∥D.G.M. and S.V.J. equally contributed to this work.

Notes

The authors declare no competing financial interest.

DOI: 10.1021/acsinfecdis.5b00117
ACS Infect. Dis. 2016, 2, 241−250

■ ACKNOWLEDGMENTS

This work was supported by the pilot project fund from the Arkansas Bioscience Institute and startup funds from the University of Arkansas to J.C. as well as Grant R56-AI093126 from the National Institute of Allergy and Infectious Disease to M.S.S. D.G.M. was supported by T32 Training Grant GM106999. E.K.M. was supported by the State Undergraduate Research Fellowships. Support was also provided by the core facilities supported by the Center for Microbial Pathogenesis and Host Inflammatory Responses (P20-GM103450) and the Translational Research Institute (UL1TR000039) through the NIH National Center for Research Resources and National Center for Advancing Translational Sciences. The content is solely the responsibility of the authors and does not necessarily represent the views of the NIH. We thank Dr. G. Keeler for assistance in the preparation of microscope slides and Drs. R. Griffin and R. Dings for providing EA-hy926 cells.

■ REFERENCES

(1) Bassetti, M., Merelli, M., Temperoni, C., and Astilean, A. (2013) New antibiotics for bad bugs: where are we? *Ann. Clin. Microbiol. Antimicrob. 12*, 22.

(2) Boucher, H. W., and Corey, G. R. (2008) Epidemiology of methicillin-resistant *Staphylococcus aureus*. *Clin. Infect. Dis. 46*, S344−S349.

(3) Chambers, H. F., and DeLeo, F. R. (2009) Waves of resistance: *Staphylococcus aureus* in the antibiotic era. *Nat. Rev. Microbiol. 7*, 629−641.

(4) Boucher, H. W., Talbot, G. H., Bradley, J. S., Edwards, J. E., Gilbert, D., Rice, L. B., Scheld, M., Spellberg, B., and Bartlett, J. (2009) Bad bugs, no drugs: no ESKAPE! An update from the Infectious Diseases Society of America. *Clin. Infect. Dis. 48*, 1−12.

(5) Römling, U., and Balsalobre, C. (2012) Biofilm infections, their resilience to therapy and innovative treatment strategies. *J. Intern. Med. 272*, 541−561.

(6) Ray, P. C., Khan, S. A., Singh, A. K., Senapati, D., and Fan, Z. (2012) Nanomaterials for targeted detection and photothermal killing of bacteria. *Chem. Soc. Rev. 41*, 3193−3209.

(7) Hamblin, M. R., and Hasan, T. (2004) Photodynamic therapy: a new antimicrobial approach to infectious disease? *Photochem. Photobiol. Sci. 3*, 436−450.

(8) Jori, G., Fabris, C., Soncin, M., Ferro, S., Coppellotti, O., Dei, D., Fantetti, L., Chiti, G., and Roncucci, G. (2006) Photodynamic therapy in the treatment of microbial infections: basic principles and perspective applications. *Lasers Surg. Med. 38*, 468−481.

(9) Berthiaume, F., Reiken, S. R., Toner, M., Tompkins, R. G., and Yarmush, M. L. (1994) Antibody-targeted photolysis of bacteria in vivo. *Bio/Technology 12*, 703−706.

(10) Kharkwal, G. B., Sharma, S. K., Huang, Y.-Y., Dai, T., and Hamblin, M. R. (2011) Photodynamic therapy for infections: clinical applications. *Lasers Surg. Med. 43*, 755−767.

(11) Zharov, V. P., Mercer, K. E., Galitovskaya, E. N., and Smeltzer, M. S. (2006) Photothermal nanotherapeutics and nanodiagnostics for selective killing of bacteria targeted with gold nanoparticles. *Biophys. J. 90*, 619−627.

(12) Norman, R. S., Stone, J. W., Gole, A., Murphy, C. J., and Sabo-Attwood, T. L. (2008) Targeted photothermal lysis of the pathogenic bacteria, *Pseudomonas aeruginosa*, with gold nanorods. *Nano Lett. 8*, 302−306.

(13) Levi-Polyachenko, N., Young, C., MacNeill, C., Braden, A., Argenta, L., and Reid, S. (2014) Eradicating group A *Streptococcus* bacteria and biofilms using functionalised multi-wall carbon nanotubes. *Int. J. Hyperthermia 30*, 490−501.

(14) Zharov, V. P., Galanzha, E. I., Shashkov, E. V., Kim, J.-W., Khlebtsov, N. G., and Tuchin, V. V. (2007) Photoacoustic flow cytometry: principle and application for real-time detection of circulating single nanoparticles, pathogens, and contrast dyes in vivo. *J. Biomed. Opt. 12*, 051503−051503−14.

(15) Galanzha, E. I., Shashkov, E., Sarimollaoglu, M., Beenken, K. E., Basnakian, A. G., Shirtliff, M. E., Kim, J.-W., Smeltzer, M. S., and Zharov, V. P. (2012) In vivo magnetic enrichment, photoacoustic diagnosis, and photothermal purging of infected blood using multifunctional gold and magnetic nanoparticles. *PLoS One 7*, e45557.

(16) Shao, J., Griffin, R. J., Galanzha, E. I., Kim, J.-W., Koonce, N., Webber, J., Mustafa, T., Biris, A. S., Nedosekin, D. A., and Zharov, V. P. (2013) Photothermal nanodrugs: potential of TNF-gold nanospheres for cancer theranostics. *Sci. Rep. 3*, 01293.

(17) Libutti, S. K., Paciotti, G. F., Byrnes, A. A., Alexander, H. R., Gannon, W. E., Walker, M., Seidel, G. D., Yuldasheva, N., and Tamarkin, L. (2010) Phase I and pharmacokinetic studies of CYT-6091, a novel PEGylated colloidal gold-rhTNF nanomedicine. *Clin. Cancer Res. 16*, 6139−6149.

(18) Pilot Study of AuroLase(tm) Therapy in Refractory and/or Recurrent Tumors of the Head and Neck; https://clinicaltrials.gov/ct2/show/NCT00848042 (accessed Oct 3, 2015).

(19) Efficacy Study of AuroLase Therapy in Subjects With Primary and/or Metastatic Lung Tumors; https://www.clinicaltrials.gov/ct2/show/NCT01679470 (accessed Oct 3, 2015).

(20) Archer, N. K., Mazaitis, M. J., Costerton, J. W., Leid, J. G., Powers, M. E., and Shirtliff, M. E. (2011) *Staphylococcus aureus* biofilms. *Virulence 2*, 445−459.

(21) Anstead, G., Cadena, J., and Javeri, H. (2014) Treatment of infections due to resistant *Staphylococcus aureus*. In *Methicillin-Resistant Staphylococcus Aureus (MRSA) Protocols*, Vol. 1085, pp 259−309 (Ji, Y., Ed.), Humana Press.

(22) Weiss, E. C., Zielinska, A., Beenken, K. E., Spencer, H. J., Daily, S. J., and Smeltzer, M. S. (2009) Impact of *sarA* on daptomycin susceptibility of *Staphylococcus aureus* biofilms in vivo. *Antimicrob. Agents Chemother. 53*, 4096−4102.

(23) Chen, J., Wang, D., Xi, J., Au, L., Siekkinen, A., Warsen, A., Li, Z.-Y., Zhang, H., Xia, Y., and Li, X. (2007) Immuno gold nanocages with tailored optical properties for targeted photothermal destruction of cancer cells. *Nano Lett. 7*, 1318−1322.

(24) Chen, J., Glaus, C., Laforest, R., Zhang, Q., Yang, M., Gidding, M., Welch, M. J., and Xia, Y. (2010) Gold nanocages as photothermal transducers for cancer treatment. *Small 6*, 811−817.

(25) Yavuz, M. S., Cheng, Y., Chen, J., Cobley, C. M., Zhang, Q., Rycenga, M., Xie, J., Kim, C., Song, K. H., and Schwartz, A. G. (2009) Gold nanocages covered by smart polymers for controlled release with near-infrared light. *Nat. Mater. 8*, 935−939.

(26) Chen, J., Yang, M., Zhang, Q., Cho, E. C., Cobley, C. M., Kim, C., Glaus, C., Wang, L. V., Welch, M. J., and Xia, Y. (2010) Gold nanocages: a novel class of multifunctional nanomaterials for theranostic applications. *Adv. Funct. Mater. 20*, 3684−3694.

(27) Zhang, Q., Li, W., Wen, L.-P., Chen, J., and Xia, Y. (2010) Facile synthesis of Ag nanocubes of 30 to 70 nm in edge length with CF_3COOAg as a precursor. *Chem.−Eur. J. 16*, 10234−10239.

(28) Beenken, K. E., Blevins, J. S., and Smeltzer, M. S. (2003) Mutation of sarA in *Staphylococcus aureus* limits biofilm formation. *Infect. Immun. 71*, 4206−4211.

(29) Postma, A., Yan, Y., Wang, Y., Zelikin, A. N., Tjipto, E., and Caruso, F. (2009) Self-polymerization of dopamine as a versatile and robust technique to prepare polymer capsules. *Chem. Mater. 21*, 3042−3044.

(30) Dreyer, D. R., Miller, D. J., Freeman, B. D., Paul, D. R., and Bielawski, C. W. (2012) Elucidating the structure of poly(dopamine). *Langmuir 28*, 6428−6435.

(31) Liebscher, J., Mrówczyński, R., Scheidt, H. A., Filip, C., Hădade, N. D., Turcu, R., Bende, A., and Beck, S. (2013) Structure of polydopamine: a never-ending story? *Langmuir 29*, 10539−10548.

(32) Ye, Q., Zhou, F., and Liu, W. (2011) Bioinspired catecholic chemistry for surface modification. *Chem. Soc. Rev. 40*, 4244−4258.

(33) Loget, G., Wood, J. B., Cho, K., Halpern, A. R., and Corn, R. M. (2013) Electrodeposition of polydopamine thin films for DNA patterning and microarrays. *Anal. Chem. 85*, 9991−9995.

DOI: 10.1021/acsinfecdis.5b00117
ACS Infect. Dis. 2016, 2, 241−250

(34) Kreibig, U., and Vollmer, M. (1995) *Optical Properties of Metal Clusters*, Vol. 25, Springer, Berlin, Germany.
(35) Lynge, M. E., van der Westen, R., Postma, A., and Stadler, B. (2011) Polydopamine − a nature-inspired polymer coating for biomedical science. *Nanoscale 3*, 4916−4928.
(36) Zhang, T., Muraih, J. K., MacCormick, B., Silverman, J., and Palmer, M. (2014) Daptomycin forms cation-and size-selective pores in model membranes. *Biochim. Biophys. Acta, Biomembr. 1838*, 2425−2430.
(37) Qiu, J., Yu, L., and Kirsch, L. E. (2011) Estimated pK_a values for specific amino acid residues in daptomycin. *J. Pharm. Sci. 100*, 4225−4233.
(38) Qiu, J., and Kirsch, L. E. (2014) Evaluation of lipopeptide (daptomycin) aggregation using fluorescence, light scattering, and nuclear magnetic resonance spectroscopy. *J. Pharm. Sci. 103*, 853−861.
(39) Ferguson, W. E., Smith, C. M., Adams, E., and Barlow, G. H. (1974) The temperature-dependent self-association of adenosine 5′-triphosphate in 0.154 M NaCl. *Biophys. Chem. 1*, 325−337.
(40) Ye, Q., Zhou, F., and Liu, W. (2011) Bioinspired catecholic chemistry for surface modification. *Chem. Soc. Rev. 40*, 4244−4258.
(41) Au, L., Zhang, Q., Cobley, C. M., Gidding, M., Schwartz, A. G., Chen, J., and Xia, Y. (2010) Quantifying the cellular uptake of antibody-conjugated Au nanocages by two-photon microscopy and inductively coupled plasma mass spectrometry. *ACS Nano 4*, 35−42.
(42) Beenken, K. E., Mrak, L. N., Griffin, L. M., Zielinska, A. K., Shaw, L. N., Rice, K. C., Horswill, A. R., Bayles, K. W., and Smeltzer, M. S. (2010) Epistatic relationships between sarA and agr in *Staphylococcus aureus* biofilm formation. *PLoS One 5*, e10790.
(43) Cassat, J. E., Dunman, P. M., McAleese, F., Murphy, E., Projan, S. J., and Smeltzer, M. S. (2005) Comparative genomics of *Staphylococcus aureus* musculoskeletal isolates. *J. Bacteriol. 187*, 576−592.
(44) Cheung, G. Y., Wang, R., Khan, B. A., Sturdevant, D. E., and Otto, M. (2011) Role of the accessory gene regulator agr in community-associated methicillin-resistant *Staphylococcus aureus* pathogenesis. *Infect. Immun. 79*, 1927−1935.
(45) Smith, E. J., Visai, L., Kerrigan, S. W., Speziale, P., and Foster, T. J. (2011) The Sbi protein is a multifunctional immune evasion factor of *Staphylococcus aureus*. *Infect. Immun. 79*, 3801−3809.
(46) Lewis, K. (2001) Riddle of biofilm resistance. *Antimicrob. Agents Chemother. 45*, 999−1007.
(47) Foster, T. J. (2005) Immune evasion by staphylococci. *Nat. Rev. Microbiol. 3*, 948−958.
(48) Cierny, G., III. (2011) Surgical treatment of osteomyelitis. *Plast. Reconstr. Surg. 127*, 190S−204S.

DOI: 10.1021/acsinfecdis.5b00117
ACS Infect. Dis. 2016, 2, 241−250